Bull. Mater. Sci., Vol. 40, No. 7, December 2017, pp. 1347–1354
https://doi.org/10.1007/s12034-017-1485-y

Synthesis and luminescence in sol–gel auto-combustion-synthesized $CaSnO_3$:Eu^{3+} phosphor

MOGES TSEGA[1,*] and FRANCIS BIRHANU DEJENE[2]

[1]Department of Physics, Bahir Dar University, Bahir Dar 3019, Ethiopia

[2]Department of Physics, University of the Free State, QwaQwa Campus, Private Bag X13, Phuthaditjhaba 9866, South Africa

*Author for correspondence (mogestsega@yahoo.com)

MS received 14 November 2016; accepted 21 February 2017; published online 14 November 2017

Abstract. Undoped and Eu-doped $CaSnO_3$ nanopowders were prepared by a facile sol–gel auto-combustion method calcined at 800°C for 1 h. The samples are found to be well-crystallized pure orthorhombic $CaSnO_3$ structure. Photoluminescence (PL) measurements indicated that the undoped sample exhibits a broad blue emission at about 420–440 nm, which can be recognized from an intrinsic centre or centres in $CaSnO_3$. Eu-doped $CaSnO_3$ showed broad blue emission centred about 434 nm, a weak peak at 465 nm and a sharp intense yellow emission line at 592 nm. The emission situated at 592 nm was assigned to the f–f transition of $^5D_0 \rightarrow {}^7F_1$ in Eu^{3+} ions. The afterglow emission and PL decay results in Eu-doped $CaSnO_3$ phosphor, which revealed that there are at least two different traps in this phosphor. From the obtained results, Eu^{3+}-doped $CaSnO_3$ phosphor could be proposed as a potential white luminescent optical material.

Keywords. $CaSnO_3$; sol–gel preparation; doping; luminescence.

1. Introduction

Perovskite-type calcium stannate ($CaSnO_3$) has received increasing attention due to its wide applications in ceramic dielectric bodies, gas and humidity sensors [1], anode materials for lithium ion batteries [2,3], photocatalysts [4], etc. As reported, only two phases of $CaSnO_3$ and Ca_2SnO_4 exist in the $CaO-SnO_2$ binary system. $CaSnO_3$, with orthorhombic perovskite structure, is composed of octahedral SnO_6, which connect to each other by sharing vertexes. Furthermore, the structure of Ca_2SnO_4, which consists of SnO_6 octahedral that are linked by edges and seven oxygen ions surrounding Ca^{2+}, exhibits an arrangement with low symmetry [5].

Recently, luminescence properties of rare-earth-cation-doped perovskite-type compounds have received considerable attention due to their abundant emission colours based on their 4f–4f or 5d–4f transitions [6]. It is well known that luminescence measurements are very sensitive to monitor variations in the chemical and structural local environment of respective luminescent ions and thus, have the potential to probe distortions of fluorescence sites. The luminescence properties of rare-earth-doped stannite crystal were reported for $CaSnO_3$:Sm^{3+}, Nd^{3+}, Er^{3+} [7], $CaSnO_3$:Eu^{3+} [8], $CaSnO_3$:Er^{3+}, Tm^{3+}, Yb^{3+} [9], $CaSnO_3$:Pr^{3+} [10], Ca_2SnO_4:Tb^{3+} [11] and M_2SnO_4:Sm^{3+} (M = Ca, Sr and Ba) [12]. Of the many rare-earth ions, Eu^{3+} ion is well known as an important activator for many different inorganic lattices producing red, green and reddish-orange light emissions [13–15]. To the best of our knowledge, the blue–yellow-emitting $CaSnO_3$:Eu^{3+} phosphor is not reported yet.

Many synthesis routes have been worked out to prepare $CaSnO_3$, such as chemical coprecipitation [16], hydrothermal method [9], sol–gel [8,17], solid-state reaction [10,18], etc. Although many papers on various kinds of synthesis were published, synthesis of $CaSnO_3$ through a sol–gel auto-combustion method is not studied extensively. It is well known that the properties of materials are related to the preparation method. In the attempt to avoid high temperature treatments and the consequent possible lack of chemical and dimensional homogeneity, the sol–gel route has become an appropriate method for the preparation of nanocrystalline materials. The benefits for preparing $CaSnO_3$ by the sol–gel auto-combustion method include the synthesis of nanosized crystalline powder with high purity at a relatively low temperature, possibility of stoichiometry-controlling process and production of homogeneous materials. In this work, we have investigated the structural, photoluminescence (PL) and thermoluminescence (TL) properties of undoped and Eu^{3+}-doped $CaSnO_3$ nanopowders prepared by sol–gel auto-combustion method. Our luminescence results show that the rare-earth-doped $CaSnO_3$ has remarkable potential for applications as an optical material in the visible emission range.

2. Experimental

Undoped and Eu^{3+}-doped $CaSnO_3$ phosphors were prepared by the sol–gel auto-combustion process. Calcium nitrate ($Ca(NO_3)_2 \cdot 4H_2O$; Sigma-Aldrich), tin chloride ($SnCl_2 \cdot 2H_2O$; Merck), europium nitrate ($Eu(NO_3)_3 \cdot 5H_2O$; Sigma-Aldrich), ethanol (C_2H_5OH; Aldrich) and citric acid ($C_8H_8O_7 \cdot H_2O$; Merck) (all $\geq$ 99.8% pure) were used as received without any further treatment. In a typical synthesis of undoped $CaSnO_3$, stoichiometric amount of the metal nitrates (Ca:Sn =1:1) were separately dissolved in 15 ml ethanol and mixed to obtain a homogeneous solution. A requisite amount of citric acid was dissolved in 10 ml ethanol and added to the solution mixture, which was followed by stirring on a magnetic stirrer at 70°C for 3 h. The molar ratio of Ca:catalyst was 1:0.75. The citric acid was used as a catalyst, which offers an excellent control over the stoichiometry and allows lower processing temperature. The Eu^{3+}-doped $CaSnO_3$ phosphor was also prepared by dissolving a specified amount of $Eu(NO_3)_3 \cdot 5H_2O$ in 15 ml ethanol and it is added dropwise in the solution, while stirring. The obtained transparent solutions were poured into silica crucibles and allowed to gel in an oven at 130°C for 2 h. The gel was then directly transferred into muffle furnace and calcined at 800°C for 1 h.

The crystal structure of the dried samples was characterized by D8 advanced X-ray diffractometer (XRD; Bruker, Germany) with CuK_α ($\lambda = 1.5418$ Å) radiation. The accelerating voltage and applied current were 40 kV and 30 mA, respectively. Data were collected at every 0.01° in angle range of 20−80° in 2θ. The UV–Vis reflectance spectra were obtained using a Parkin Elmer (lambda 950) spectrometer with 150 mm InGaAs integrating sphere accessory. Luminescence spectra and the lifetime measurements were performed at room temperature by using Hitachi F-7000 fluorescence spectrophotometer. Thermally stimulated luminescence (TSL) glow curves and emission spectra were recorded using PC-controlled TL dosimeter reader with charge coupled device (CCD) spectrometer (TL 1009I). Particle size analysis, crystallinity and lattice spacing of the samples were studied using transmission electron microscope (TEM; JEOL, JEM-2010F) and high-resolution transmission electron microscope (HRTEM; JEOL JEM-3010F) operated at 200 kV. Elemental composition was carried out by energy dispersive spectroscopy (EDS) attached to TEM. All the measurements were conducted at room temperature.

3. Results and discussion

3.1 *XRD analysis*

XRD patterns of $CaSnO_3$ and 3 mol% Eu^{3+}-doped $CaSnO_3$ nanoparticles are shown in figure 1. XRD was used to investigate phase purity and crystallization of the prepared nanoparticles. The observed patterns indicate that the prepared samples are single orthorhombic phase. The peaks

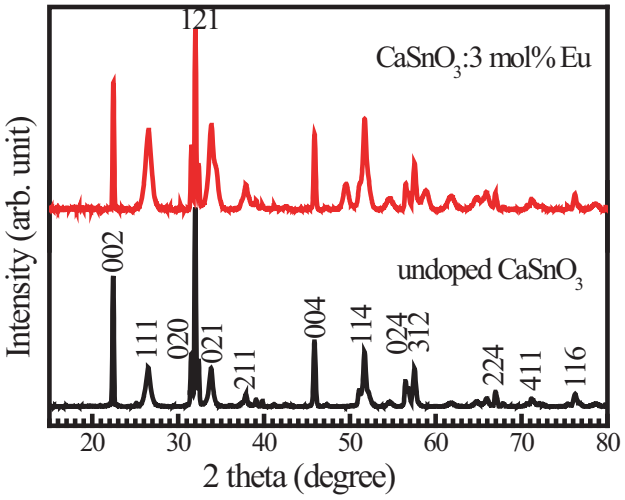

Figure 1. XRD patterns for undoped and Eu-doped $CaSnO_3$ phosphor calcined at 800°C for 1 h.

correspond to the (002), (111), (020), (121), (021), (211), (004), (114), (024), (312), (224), (411) and (116) $CaSnO_3$ planes, which are consistent with the JCPDS (77-1797). The preferred orientation was along (121) planes. This XRD result is also in good agreement with the diffraction pattern of $CaSnO_3$ single phase, reported by Pang *et al* [15] and Zhang *et al* [9]. No characteristic peaks of any impurity phase were observed suggesting that doping of Eu^{3+} ions has not distorted the crystal structure of $CaSnO_3$. It is reported that calcium stannate formation starts at temperature ~900°C and proceeds up to 1500°C by the solid-state reaction method [13]. However, our sol–gel auto-combustion method provided a pure $CaSnO_3$ phase at 800°C. This may be due to the high activity among the nitrate and chloride precursors in the sol–gel process to form the final product under calcination.

Table 1 lists the values of full-width at half-maximum (FWHM), crystallite size and lattice constants of the undoped and Eu-doped $CaSnO_3$ samples. Crystallite size of samples was calculated using most intense peak (121) of undoped and Eu-doped $CaSnO_3$ nanoparticles. The FWHM of the (121) peak was 0.2065 for undoped and 0.2362 for Eu-doped $CaSnO_3$. The average crystallite size (D) was estimated based on the FWHM of (121) diffraction peak using Debye–Scherrer's equation as follows [19]:

$$D = \frac{0.9\lambda}{\beta \cos\theta}, \tag{1}$$

where D is the crystallite size, λ the X-ray wavelength, β the FWHM in radian 2θ of a reflection located at 2θ and θ the Bragg diffraction angle. The crystallite size slightly decreased from 36.85 to 34.92 nm for the undoped and 3 mol% Eu^{3+}-doped $CaSnO_3$ nanopowders, respectively. The lattice constants (i.e., a, b and c) were also calculated from the lattice spacing of (002) and (121) peaks in accordance with the Bragg

Table 1. Peak position, FWHM, estimated crystallite size and lattice constants of undoped and Eu-doped $CaSnO_3$ nanopowders.

Sample	(121) plane (2θ)	FWHM (121) plane	Crystallite size (nm)	Lattice constant (Å)		
				a	*b*	*c*
Undoped $CaSnO_3$	31.997	0.2165	36.85	5.4941	5.6760	7.9280
Eu-doped $CaSnO_3$	32.015	0.2362	34.92	5.5008	5.6725	7.9166

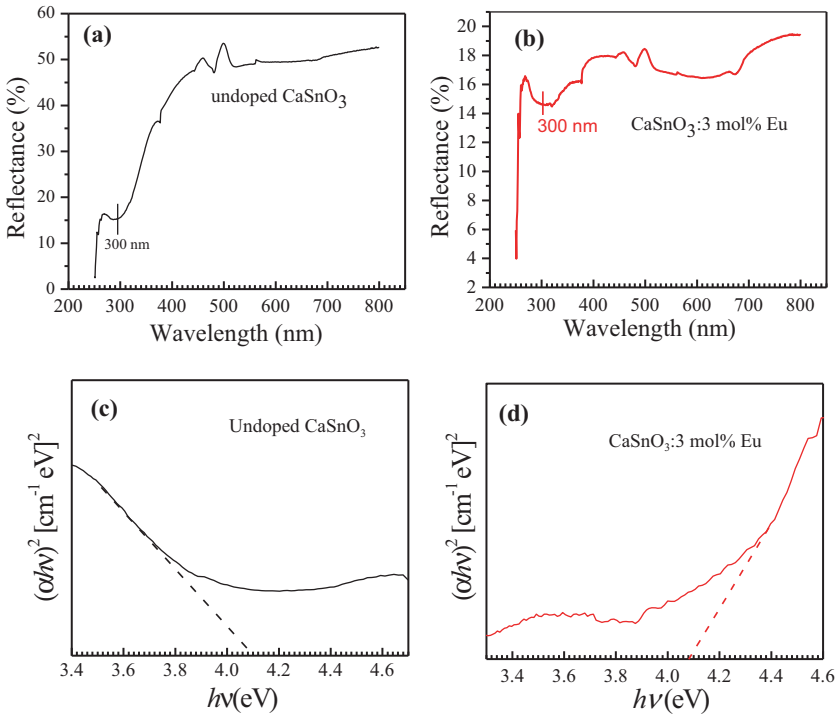

Figure 2. UV–visible reflectance spectra of (**a**) undoped $CaSnO_3$, (**b**) Eu-doped $CaSnO_3$ and the corresponding plot of $(\alpha h\nu)^2$ *vs.* $h\nu$ of (**c**) undoped and (**d**) Eu-doped $CaSnO_3$ nanopowders measured at room temperature.

equation for the orthorhombic lattice structure ($a \neq b \neq c$) using equation (2):

$$\frac{1}{d_{hkl}^2} = \frac{h^2}{a^2} + \frac{k^2}{b^2} + \frac{l^2}{c^2}. \tag{2}$$

Here d_{hkl} is the spacing between the planes corresponding to Miller indices h, k, l and a, b, c are the lattice constants. The value of the lattice parameters of $a = 5.4941$ Å, $b = 5.6760$ Å and $c = 7.9280$ Å for undoped $CaSnO_3$; and $a = 5.5008$ Å, $b = 5.6725$ Å and $c = 7.9166$ Å for Eu-doped $CaSnO_3$. The calculated lattice constants are close to the literature values [20,21]. The ionic size of Eu^{3+} cation is about 0.95 Å (effective ionic radius, IR), whereas it is 0.99 Å for Ca^2 [22]. IR of the dopant in the host material is used to determine its sites. From the XRD analysis, it was observed that the introduction of an activator (Eu^{3+}) did not influence the crystal structure of the phosphor matrix, hence, the change in the lattice constants was almost negligible. This may be due to the low ionic radii mismatch between the dopant and the substituted calcium ion.

3.2 *Optical properties*

Figure 2a and b shows the room-temperature reflection spectra of the undoped and 3 mol% Eu^{3+}-doped $CaSnO_3$ nanoparticles recorded in the wavelength range of 200–800 nm. It can be seen that both samples have much lower reflectance at shorter wavelengths and a broad absorption band in the UV region around 300 nm, which corresponds to the transition from the $^7F_0$ ground state to the charge transfer state due to the oxygen–cation interaction [23]. To calculate the optical band-gap energy (E_g) of the synthesized $CaSnO_3$ nanoparticles, we assume that the absorption coefficient (α)

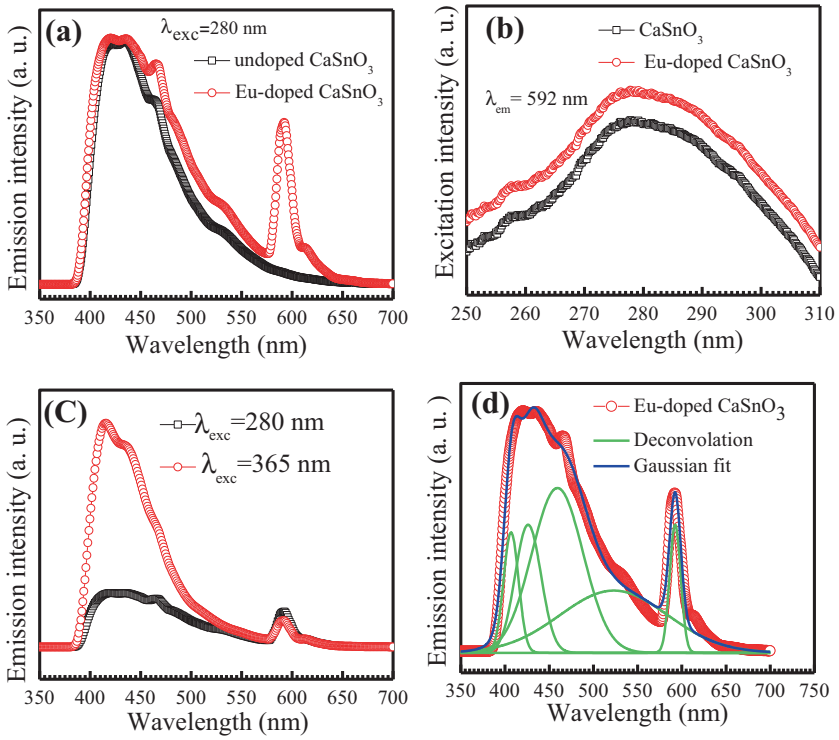

Figure 3. (**a**) Room temperature PL emission and (**b**) excitation spectra of undoped and Eu-doped $CaSnO_3$ nanopowders, (**c**) emission spectra of Eu-doped $CaSnO_3$ nanopowder under excitations at $\lambda_{exc} = 280$ and 365 nm and (**d**) the deconvolution of the emission spectrum for Eu-doped $CaSnO_3$ sample at $\lambda_{exc} = 280$ nm.

is given by the following relation [24]:

$$\alpha = \frac{(1-R)^2}{2R}, \tag{3}$$

where R is the reflectance (%). In fact, orthorhombic structure of $CaSnO_3$ has a direct band gap, and in this case, the absorption edge for a direct band transition is analysed by the following relation [25]:

$$[\alpha h\nu] = A\left(h\nu - E_g\right)^{1/2}, \tag{4}$$

where $h\nu$ is the photon energy and A is a proportionality constant. The values of the direct band gap were determined by extrapolations of the linear regions of the plots to zero absorption ($(\alpha h\nu)^2 = 0$). The E_g values were 4.08 eV (figure 2c) and 4.10 eV (figure 2d) for undoped and Eu-doped $CaSnO_3$ nanoparticles, respectively. The obtained E_g values of undoped and Eu-doped $CaSnO_3$ nanoparticles are in agreement with the E_g values of $CaSnO_3$ microcube prepared by hydrothermal process [26].

Figure 3a shows the PL emission spectra of the undoped and Eu-doped $CaSnO_3$ nanoparticles excited by 280 nm at room temperature. The PL emission of undoped $CaSnO_3$ phosphor contains broad blue emission at about 420–440 nm centred at 434 nm. The possible defects that can contribute to PL characteristic are oxygen vacancies, and it is the transitions of electrons from the defect energy level to the valence band, possessing the wavelength between 400 and 500 nm located in the visible light region [13]. The high-temperature calcination gives rise to oxygen vacancies, which are at least partially charge compensated by the creation of reduced Sn^{n+} sites ($n < 4$) [13]. The PL spectrum of 3 mol% Eu-doped $CaSnO_3$ nanoparticles has a strong and broad blue band peaks centred at 420, 437 and 465 nm, and an intense sharp yellow band centred at about 592 nm. The emission at 465 nm is attributed to the electric dipole allowed $^5D_2 \rightarrow {}^7F_0$ transitions of Eu^{3+} ions [27]. A sharp band at 592 nm is assignable due to the characteristic transitions of Eu^{3+} ions between $^5D_0 \rightarrow {}^7F_1$ energy level [28]. It is widely understood that the magnetic dipole transition $^5D_0 \rightarrow {}^7F_1$ is dominant when Eu^{3+} ions in the crystal lattice occupies a site with inversion symmetry [13]. Figure 3b shows the excitation spectra of undoped and Eu-doped $CaSnO_3$ nanpowders at room temperature. The excitation spectra were measured by monitoring the emission wavelength at 592 nm. Both samples exhibited broad peak in the range of 270–300 nm centred at around 280 nm. This excitation peak can be attributed to the intrinsic defects among the constituents of $CaSnO_3$ matrix. Figure 3c shows the emission spectra of Eu-doped $CaSnO_3$ phosphors under excitation at 280 and 365 nm. The blue luminescence emission for excitation at $\lambda_{exc} = 280$ nm, which is much weaker and

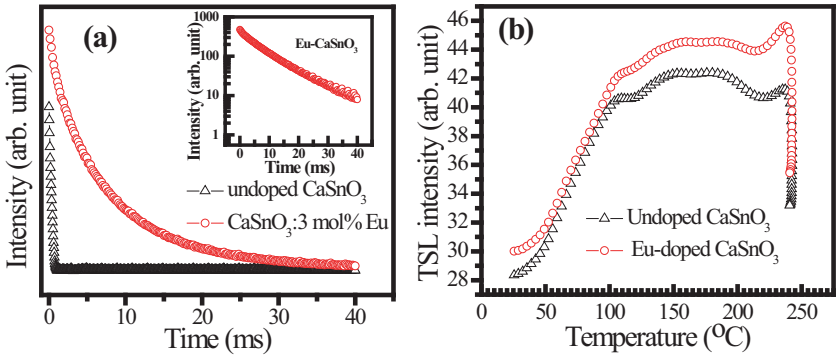

Figure 4. (**a**) Luminescence decay time profile and (**b**) TSL glow curve of the undoped and 3 mol% Eu^{3+}-doped $CaSnO_3$ phosphor calcined at 800°C for 1 h.

broader than the emission peak for excitation at $\lambda_{exc} = 365$ nm. Upon excitation $\lambda_{exc} = 280$ nm, however, the emission intensity at 592 nm originated from Eu^{3+} ions is slightly increased than the emission at the excitation wavelength $\lambda_{exc} = 365$ nm. The increase in emission intensity after $\lambda_{exc} = 280$ nm excitation, confirms the influence of the excitation wavelength on the emission of Eu^{3+} ions. Therefore, different emission spectra can be obtained by adjusting the excitation wavelengths. Figure 3d shows the Gaussian fitting and the de-convoluted PL emission spectrum for the 3 mol% Eu-doped $CaSnO_3$ phosphor. Five defect-related peaks are observed at 420, 437, 465, 525 and 592 nm.

The decay time curves for the undoped and $CaSnO_3$:3 mol% Eu^{3+} samples calcined at 800°C for 1 h are shown in figure 4a. Measurements of luminescence decay kinetics were carried out by monitoring the $\lambda_{em} = 592$ nm emission line upon excitation at $\lambda_{ex} = 280$ nm. The figure shows that both samples exhibit completely different trends of PL decay profiles. The undoped sample showed a sharp drop and difficult to fit. However, Eu-doped $CaSnO_3$ phosphor showed quite long decay time. The inset in figure 4a shows the luminescence decay curve in semi-log plot for Eu-doped $CaSnO_3$ phosphor. The semi-log plot helps to find that how many processes are involved in the decay process. The decay curve can be fitted by the third-order exponential function as [29]:

$$I(t) = A_1 \exp\left(\frac{-t}{\tau_1}\right) + A_2 \exp\left(\frac{-t}{\tau_2}\right) + A_3 \exp\left(\frac{-t}{\tau_3}\right), \tag{5}$$

where $I(t)$ represents the phosphorescence intensity; A_1, A_2 and A_3 are constants; t represents the time, τ_1, τ_2 and τ_3 are decay times for the exponential components. The triexponential decay indicates that more than one decay channel is involved in the total decay process. The decay is characterized by three components, namely the fast, the intermediate and the slow components for which the decay constants were found to be $\tau_1 = 0.63 \pm 0.03$, $\tau_2 = 4.64 \pm 0.22$ and $\tau_3 = 10.64 \pm 0.32$ ms, respectively. Larger the value of τ, the longer the afterglow is implied. The initial rapid decay with the time constant $\tau_1 = 0.63 \pm 0.03$ ms is attributed to the non-radiative lifetime due to the short survival time of an electron in Eu^{3+}. The intermediate transitional decay ($\tau_2 = 4.64 \pm 0.22$ ms) and slow-decaying process ($\tau_3 = 10.64 \pm 0.32$ ms) is attributed to the radiative recombination at the $CaSnO_3$ nanopowders. The increase in the radiative life time indicates the decrease in the disorder around Eu^{3+} ions. The radiative recombination might be the capture of Eu^{3+} by a deep trap energy centre. This indicates the presence of persistent luminescence [8]. The average lifetime in case of a non-exponential with three components can be calculated using the following equation:

$$\tau_{av} = \frac{A_1\tau_1^2 + A_2\tau_2^2 + A_3\tau_3^2}{A_1\tau_1 + A_2\tau_2 + A_3\tau_3}. \tag{6}$$

The calculated average decay time of Eu^{3+}-doped $CaSnO_3$ nanopowder is found to be 9.12 ms. This decay value is longer than the PL decay behaviour of Eu^{3+}-doped $CaSnO_3$ nanophosphor prepared by the solid-state reaction method [30]. The quantum efficiency is the ratio of effective and radiative lifetimes that the number of photons created and divided by the number of photons absorbed. Therefore, the quantum efficiency of overall luminescence can be calculated using the following formula [31]:

$$\eta = \frac{\tau_{av}}{\tau_R} \times 100\%, \tag{7}$$

where τ_{av} and τ_R are the average and radiant lifetimes for Eu-doped phosphor, respectively. The estimated quantum efficiency of the $CaSnO_3$:3 mol% Eu sample was ~60%. The achieved quantum efficiency is larger than the quantum efficiency estimated in Eu^{3+}-doped $GdPO_4$ nanoparticles [32].

Figure 4b shows the typical TL glow curves of undoped and 3 mol% Eu^{3+}-doped $CaSnO_3$ nanoparticles. The glow curves were recorded at a heating rate of 1°C s^{-1} and irradiated at UV source. In optical-stimulation process, the UV irradiated powder excited with blue photons and the output was recorded after 20 min illumination. As shown in figure 4b,

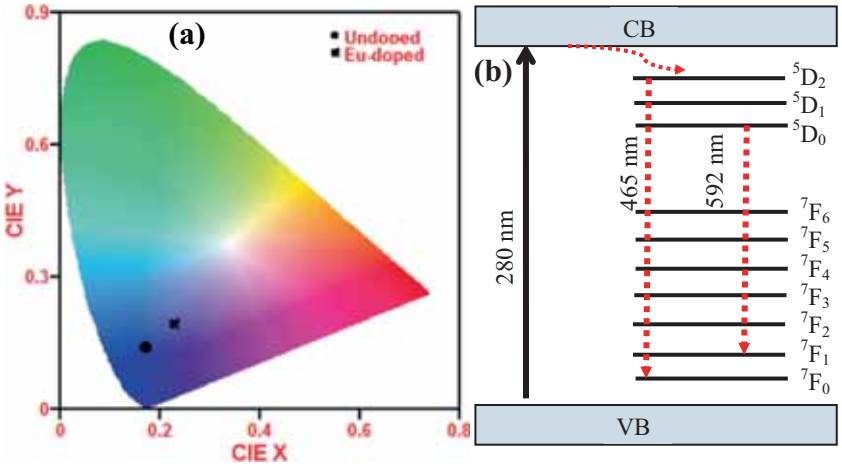

Figure 5. (**a**) CIE colour coordinates for the undoped and 3 mol% Eu-doped $CaSnO_3$ phosphors (λ_{exc} = 280 nm) and (**b**) proposed emission mechanism pathways in $CaSnO_3$:3 mol% Eu^{3+} nanophosphor.

the shapes of the TL spectra are broad and not appear as a single peak, indicating the presence of various traps. TL glow curve of the undoped $CaSnO_3$ sample showed a broad peak in the range of 125–196°C and a slightly intense peak at 236°C, where the trapping states are primarily assigned to natural defects of the host. The broad nature of the peak may be attributed to the overlap of various peaks with a close distribution of their trap depths. On the other hand, TL glow curve of Eu-doped $CaSnO_3$ sample showed an intense peak at 236°C. Both undoped and doped samples revealed the same glow curve structure, but intensity is found to increase for Eu-doped $CaSnO_3$ sample in comparison to the TL spectrum of the undoped $CaSnO_3$ sample. This change in the relative intensity of the peaks is attributed to the change in the population of the luminescent/trapping centres due to the introduction of Eu^{3+} ions into the $CaSnO_3$ host. As the light falls on the sample, the electrons are released from the traps thus, increasing the output signal.

Figure 5a shows the International Commission on Illumination (CIE) chromaticity diagram of undoped and Eu-doped $CaSnO_3$ nanopowders. The calculated CIE coordinates of the undoped and Eu-doped $CaSnO_3$ nanophosphor were found to be $(x, y) = (0.168, 0.135)$ and $(x, y) = (0.227, 0.196)$, respectively. These coordinates correspond to blue for the undoped sample, and bluish-yellow light emission for Eu-doped $CaSnO_3$ nanophosphor. Figure 5b shows the proposed emission mechanism in $CaSnO_3$:3mol% Eu^{3+} phosphor. It is well known that trapping centres play an essential role for photostimulated and thermostimulated phosphors [33].

3.3 *TEM analysis*

The crystallization behaviour of the heat-treated Eu-doped $CaSnO_3$ nanoparticles was also studied by TEM and HRTEM to determine particle morphology, crystallite size, as well as homogeneity at nanometer scale. Figure 6a and b show the TEM images of Eu-doped $CaSnO_3$ nanopowder after calcined at 800°C for 1 h. They consist of quasi-spherical agglomerated nano-scaled particles about 10 nm in diameter. From the distance between the adjacent lattice fringes, the lattice plane on the nanoparticles can be assigned. Figure 6c shows the HRTEM image of single nanoparticle of the corresponding sample. It clearly shows an ordered fringes spaced at 0.28 nm corresponding to the crystalline (121) plane of the $CaSnO_3$, which is the strongest crystallographic plane [3]. This value is in agreement with the highest intensity peak in XRD pattern (figure 1). Figure 6d shows the selected area electron diffraction (SAED) image of 3 mol% Eu^{3+}-doped $CaSnO_3$ phosphor, displaying obvious ringpatterns made of bright dots. These rings indicate the polycrystalline nature of the Eu-doped $CaSnO_3$ nanoparticles. The corresponding EDX spectrum of the sample in figure 6e shows that the crystal is composed of Ca, Sn and O atoms, and no other impurity is detected. In this spectrum, signals corresponding to C and Cu arise from the TEM grid.

4. Conclusions

Undoped blue–yellow emitting phosphor and $CaSnO_3$:3mol% Eu^{3+} phosphor powders with orthorhombic structure and quasi-spherical particles were successfully prepared by a sol–gel auto-combustion method. The blue–yellow emissions and mechanism were also carefully studied. The broad blue PL emission peaks at 420–440 nm were obtained for the undoped sample. Eu-doped $CaSnO_3$ phosphor, on the other hand, showed broad emission at about 420–440 nm, weak intensity at 465 nm and sharp yellow emission centred at 592 nm. The emission lines at 465 and 592 nm were assigned to the f–f transition of $^5D_2 \rightarrow {}^7F_0$ and $^5D_0 \rightarrow {}^7F_1$ in Eu^{3+} ions,

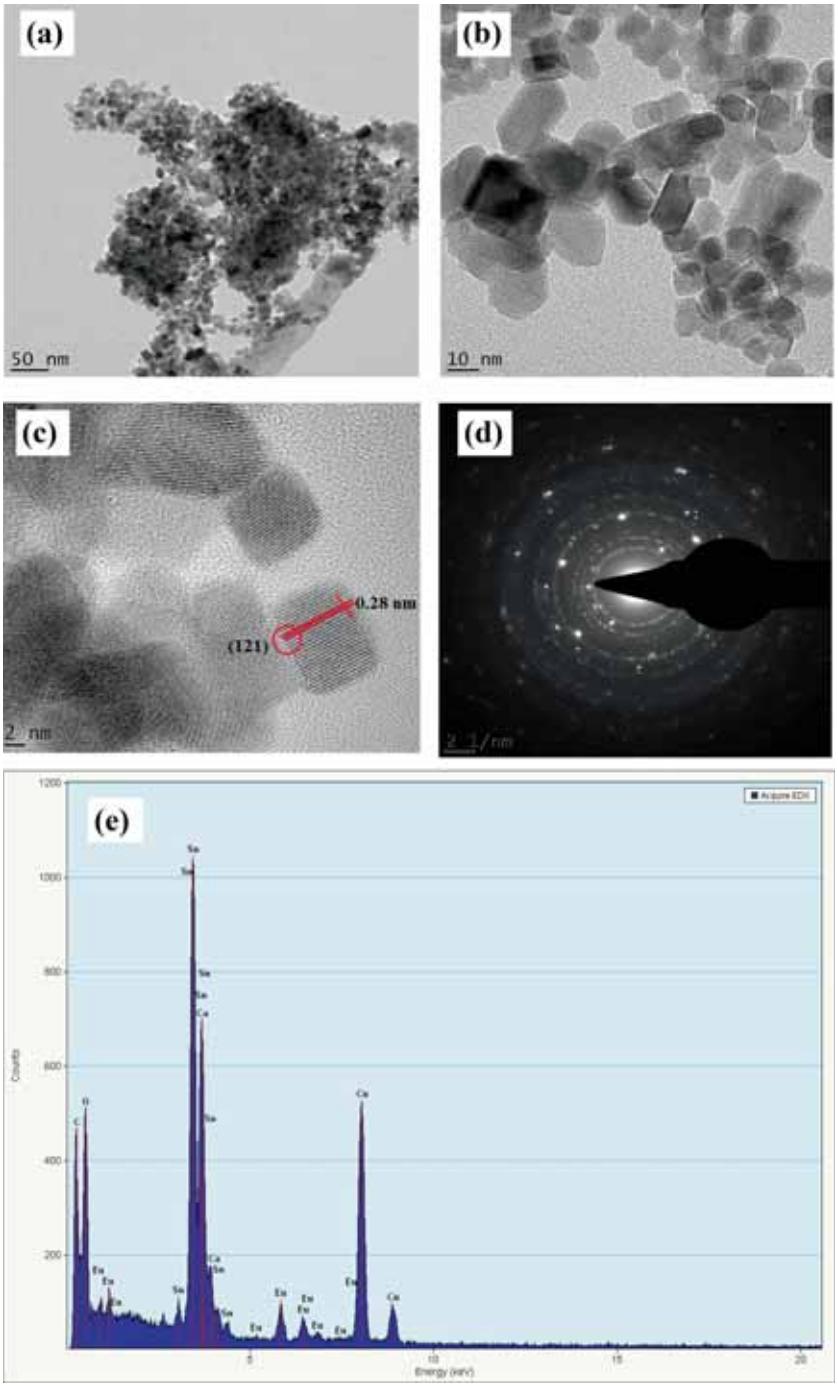

Figure 6. TEM images of Eu-doped $CaSnO_3$ phosphor: (**a**, **b**) TEM; (**c**) HRTEM; (**d**) SAED and (**e**) EDX.

respectively. The TL and luminescence decay results in the Eu-doped sample, which revealed that there are at least two different traps in this phosphor. The mixture of blue and yellow luminescence could give white colour in $CaSnO_3$:Eu^{3+} phosphor under UV excitation.

Acknowledgements

This work is funded by the University of the Free State, Division of Postgraduate Research Development, South Africa (grant no. LHIK500).

References

[1] Cheng H and Lu Z 2008 *Solid State Sci.* **10** 1042
[2] Mouyane M, Womes M, Jumas J C, Fourcade J O and Lippens P E 2011 *J. Solid State Chem.* **184** 2877
[3] Li L, Peng S, Wang J, Cheah Y L, Teh P, Ko Y, Wong C and Srinivasan M 2012 *Appl. Mater. Interfaces* **4** 6005
[4] Singh M K, Hong J W, Karan N K, Jang H M, Katiyar R S, Redfern S A T *et al* 2010 *J. Phys. Condens. Matter.* **22** 095901
[5] Chen X Y, Ma C, Bao S P and Zhang H Y 2010 *J. Alloys Compd.* **497** 354
[6] Sun J Y, Zeng J H, Sun Y N and Du H Y 2012 *J. Alloys Compd.* **540** 81
[7] Gordo V O, Arslanli Y T, Canimoglu A, Ayvacikli M, Gobato Y G, Henini M *et al* 2015 *Appl. Radiat. Isot.* **99** 69
[8] Saha S, Das S, Ghorai U K, Mazumder N, Ganguly D and Chattopadhyay K K 2015 *J. Phys. Chem. C* **119** 16824
[9] Pang X L, Jia C H, Li G Q and Zhang W F 2011 *Opt. Mater.* **34** 234
[10] Stanulis A, Katelnikovas A, Van Bael M, Hardy A, Kareiva A and Justel T 2016 *J. Lumin.* **172** 323
[11] Jin Y, Hun Y, Chen L, Wang X, Ju G and Mu Z 2013 *J. Lumin.* **138** 83
[12] Stanulis A, Katelnikovas A, Enseling D, Dutczak D, Sakirzanovas S, Bael M V *et al* 2014 *Opt. Mater.* **36** 1146
[13] Canimoglu A, Guinea J G, Karabulut Y, Ayvacikli M, Jorge A and Can N 2015 *Appl. Radiat. Isot.* **99** 138
[14] Fu Z, Yang H K, Moon B K, Choi B C and Jeong J H 2009 *J. Lumin.* **129** 1669
[15] Zhang J, Chen B, Liang Z, Li X, Sun J, Cheng L *et al* 2014 *J. Alloys Compd.* **612** 204
[16] Chen S X, Ma C, Bao S and Zhang H 2010 *J. Alloys Compd.* **497** 354
[17] Ju Z, Zhang S, Gao X, Tang X and Liu W 2011 *J. Alloys Compd.* **509** 8082
[18] Berbenni V, Milanese C, Bruni G, Girella A and Marini A 2015 *Thermochim. Acta* **608** 59
[19] Otsubo K, Haraguchi T, Sakata O, Fujiwara A and Kitagawa H 2012 *J. Am. Chem. Soc.* **134** 9605
[20] Mountstevens E H, Attfield J P and Redfern S A T 2005 *J. Phys. Condens. Matter* **15** 8315
[21] Goto K, Nakachi Y and Ueda K 2008 *Thin Solid Films* **516** 5885
[22] Shannon R D and Prewitt C T 1969 *Cryst. Chem.* **25** 925
[23] Chen Y C, Chang Y H and Tsai B S 2005 *Opt. Mater.* **27** 1874
[24] Simmons E L 1975 *Appl. Opt.* **14** 1380
[25] Yoldas B E and Partlow D P 1985 *Thin Solid Films* **129** 1
[26] Wang W J, Bi J H, Wu L, Li Z H and Fu X Z 2009 *Scr. Mater.* **60** 186
[27] Yanes A C, Del-Castillo J, Méndez-Ramos and Rodríguez V D 2011 *J. Nanopart Res*. **13** 7295
[28] Ashtaputre S S, Nojima A, Marathe S K, Matsumura D, Ohta T, Tiwari R *et al* 2008 *J. Phys. D Appl. Phys.* **41** 015301
[29] Yoon S, Otal E H, Maegli A E, Karvonen L, Matam S K, Ebbinghaus S G *et al* 2014 *J. Alloys Compd.* **613** 338
[30] Zhang J, Chen B, Liang Z, Li X, Sun J, Cheng L and Zhong H 2014 *J. Alloys Compd.* **612** 204
[31] Sobczyk M, Szymański D, Guzik M and Legendziewicz J 2016 *J. Lumin.* **169** 794
[32] Hassairi M A, Hernández A G, Kallel T, Dammak M, Zambon D, Chadeyron G *et al* 2016 *J. Lumin.* **170** 200
[33] Jia D, Jia W, Evans D R, Dennis W M, Liu H, Zhu J *et al* 2000 *J. Appl. Phys.* **88** 3402